JOURNAL OF SPACECRAFT AND ROCKETS
Vol. 32, No. 3, May–June 1995

Flight Mass-Spectrometer Calibration in a High-Velocity Atomic-Oxygen Beam

Jon B. Cross*
Los Alamos National Laboratory, Los Alamos, New Mexico 87545
Steven L. Koontz†
NASA Johnson Space Flight Center, Houston, Texas 77058
and
Don E. Hunton‡
U. S. Air Force Phillips Laboratory, Hanscomb Air Force Base, Massachusetts 01713

Calibration and characterization of the quadrupole mass-spectrometer component of the Evaluation of Oxygen Interactions with Materials III space-flight experiment are reported in this paper. A high-velocity atom beam system was used to characterize the response of the flight mass spectrometer to high-velocity oxygen atoms (0.8 to 2.5 eV). The response factor based on oxygen atom flux in the high-velocity beam was found to be logarithmically dependent on the exposure history of the instrument, i.e., the calibration factor was logarithmically dependent on atomic oxygen fluence. This dependence was independent of the background pressure over the range between 10^{-6} and 10^{-4} Torr. Subsequent contamination of the instrument restored the instrument sensitivity to the original value before exposure to atomic oxygen. Carbon dioxide, carbon monoxide, and water were observed in the mass spectrometer whenever high-velocity oxygen atoms were present. The intensity of reaction products caused by interaction of atomic oxygen with contaminated surfaces within the instrument decreases with increasing atomic oxygen fluence, whereas O_2 resulting from recombination of atomic oxygen on surfaces increases with fluence.

Nomenclature

k = Boltzmann constant
M = atomic mass
T = temperature, K
v = velocity
W = watt
ρ^i = partial number density
ϖ_i = most probable thermal velocity of species i

I. Introduction

THE Evaluation of Oxygen Interactions with Materials III (EOIM-III) space-flight experiment was flown on STS-46 and has been described[1,2] at length previously. An important objective of the flight is quantitative measurement of material reactivities with atomic oxygen (AO) in the low Earth orbit (LEO) environment, for which estimates of AO flux and fluence are needed. Previous flight experiments aimed at evaluating interactions of materials with AO have relied on the MSIS atmospheric model[3] to predict atom fluxes[4–7] on experiment surfaces. The MSIS model is based, in part, on satellite drag measurements, which show[3] a characteristic standard deviation of ±15% to ±18%. Direct measurements of ram flux during EOIM-III will supplement MSIS-86 predictions and improve the accuracy of atom flux and fluence estimates.

The calibration and use of satellite mass spectrometers has been discussed at length by Nier et al.[8,9] in connection with the Atmospheric Explorer Satellite series (an important source of data for the MSIS model). An ideal calibration system should produce a perfect replica of the LEO environment with respect to both the flux of various species and their relative velocity with respect to the spacecraft. A reliable technique for producing high-velocity, high-flux oxygen beams with known absolute flux and velocity is important for a successful calibration, but is not sufficient in itself. The influence of any differences between the LEO environment and the calibration-system environment must be evaluated, and the effect of those differences on the calibration results determined.

Conventional electron impact mass spectrometers (such as the EOIM-III mass spectrometer) produce an output signal proportional to the number density of gaseous species in the ionizing electron beam. Nier and Ballenthin[8] distinguish between open and closed ion sources for satellite mass spectrometers. In closed ion sources, high-velocity ambient gas is first thermalized by surface scattering/reaction processes in an accommodation or collision chamber so that only thermalized gaseous species, which have experienced many surface collisions, can enter the ion source. In contrast, the gaseous species in an open-source ionizer consists of both high-velocity ambient gases and thermalized gases formed by scattering/reaction processes in the mass spectrometer itself. The relative abundance of high-velocity and thermalized beam species and reaction products depends on the details of ion-source design. The EOIM-III mass spectrometer is an open-source instrument, and as a result, atomic oxygen ram flux measurements can be effected by the development of "ram density" in the ion source (i.e., an enhanced density of various beam species resulting from thermalization in the ion formation region), as will be discussed in Sec. II.C.

II. Apparatus and Methods

In this section of the paper, we present 1) the calibration-system configuration and experimental methods and 2) data reduction and calculational methods.

A. Calibration System Configuration

The overall configuration of the calibration system is shown in Fig. 1, and Fig. 2 shows the details of the calibration concept. The high-velocity AO beam system has been described, as has the quadrupole-type flight mass spectrometer[2,10,11] shown schematically in Figs. 3a and 3b. Briefly, the high-velocity oxygen atom beam is generated by supersonic nozzle expansion of a high-temperature cw-laser-sustained discharge. The working gas is typically a mixture of molecular oxygen with an inert gas such as argon, neon, or

Received April 6, 1994; revision received July 20, 1994; accepted for publication Oct. 26, 1994.

*Senior Staff. Member AIAA.
†Aerospace Technologist, Materials. Member AIAA.
‡Atmospheric Physicist. Member AIAA.

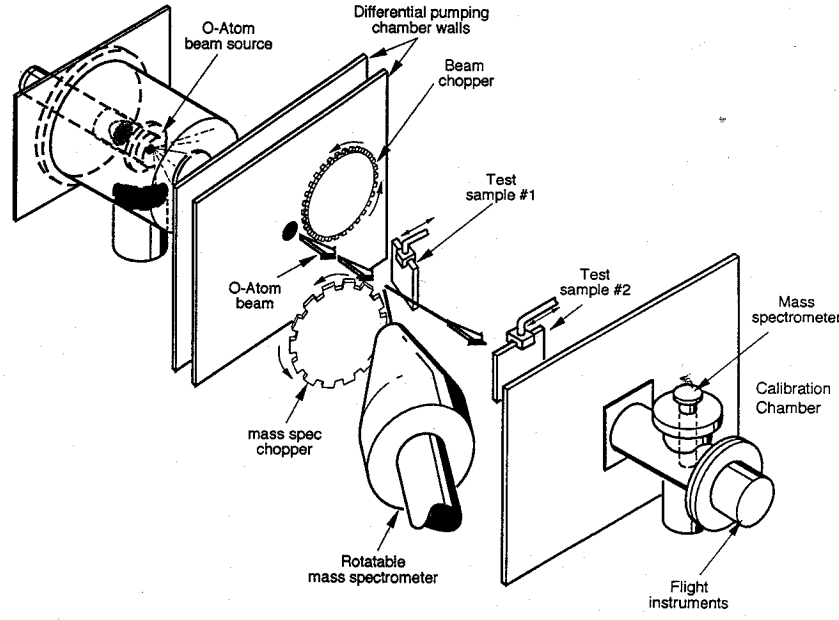

Fig. 1 Schematic diagram of molecular-beam apparatus.

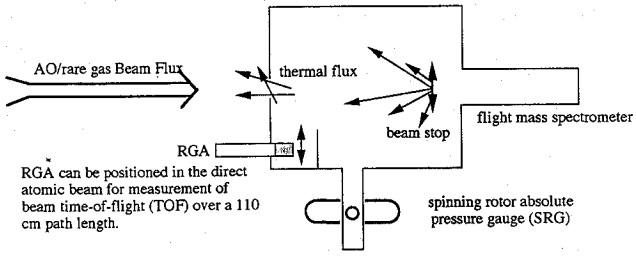

Fig. 2 Schematic diagram of AO absolute flux calibration equipment.

helium-neon mixture at a pressure of about 2000 Torr in the discharge region. With the CO_2 laser delivering about 1300 W to the plasma and the plasma plugging the nozzle orifice, the rare-gas–oxygen mixture is heated by the plasma to form a 98–99%-dissociated neutral atomic oxygen beam having a stagnation temperature of 6000 to 12,000 K, depending upon the rare gas used. Extensive measurements of the charged-particle content of the beam using the flight mass spectrometer showed that the flux of charged particles was at most 10^{-6} times that of the neutral atoms (the limit of the instrument's sensitivity). The high-pressure operation of the source causes very rapid ion-electron recombination and collisional relaxation of any excited-state neutrals.[12] The oxygen atoms in the high-velocity beam are predominantly in the O^3P electronic ground state when one employs argon as the inert gas. The high-velocity atom beam crosses the main vacuum chamber, which contains various beam diagnostic instruments (Fig. 1), and then enters a small, differentially pumped vacuum chamber (calibration chamber) via a 1.27–cm-diameter aperture (Fig. 2). During beam operation, the pressure in the main vacuum chamber is typically 2×10^{-6} Torr, and the calibration-chamber pressure is typically $(2–3) \times 10^{-5}$ Torr when the turbopump is valved off.

The EOIM-III mass spectrometer, coaxial with the atom beam, is mounted at the end of the accommodation chamber (Fig. 2) so that the well-defined AO–rare-gas beam is swallowed by the mass spectrometer. In this configuration, the high-velocity atom beam impinges directly on the EOIM-III mass-spectrometer ion source as it will during ram flux measurements in LEO. The calibration chamber can be isolated from its turbomolecular pump by a gate valve in order that accurate absolute pressure measurements can be taken. The accommodation chamber is equipped with a movable mass-spectrometer beam flag and a molecular-drag vacuum-gauge head both located near the EOIM-III mass-spectrometer ion source. The beam stop (Fig. 2) is employed to correct for the remaining ambient

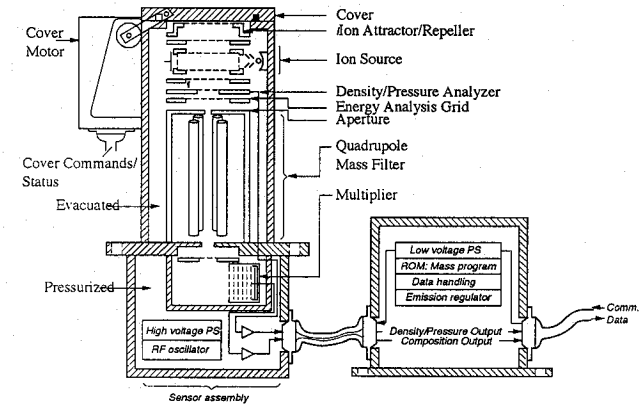

a) Schematic diagram

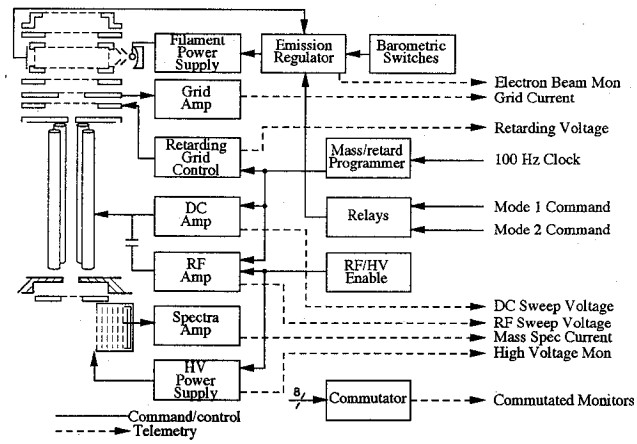

b) Block diagram of electronics

Fig. 3 Flight mass spectrometer.

background in the calibration chamber, i.e., spectra taken with the beam stop blocking the beam from reaching the instrument are subtracted from the direct-beam spectra to obtain the net effect of the direct beam alone. The distance from the beam source to the accommodation-chamber aperture is 90 cm; the distance from the beam-source nozzle to the EOIM-III mass-spectrometer ion source is 133 cm.

A schematic diagram of the flight mass-spectrometer is shown in Fig. 3a, and a block diagram of the electronics is shown in Fig. 3b. In the schematic diagram, note the large-volume ionization region along with an equally large-diameter (≈1 cm) opening into the ion source region. The entrance aperture into the quadrupole mass analysis region is, however, much smaller in diameter (≈2 mm). These facts are important in estimating the ratio of ion signal arising from ionization of thermalized species within the source to that from ionization of the direct flythrough flux, viz., the direct flythrough ion current is only about 4% that of the thermalized signal. In addition, this small-diameter entrance aperture appears to be involved in fluence-dependent sensitivity changes. The electronics block diagram in Fig. 3b shows that the emission current is trap-regulated and provides a constant ionizing electron current.

B. Characterization of the High-Velocity Beam

Characterization of the high-energy beam was conducted as follows. High-resolution time-of-flight (TOF) velocity analysis data were collected using a movable residual gas-analyzer (RGA) of the quadrupole type in single-ion monitoring mode as the beam detector, with a beam flight path of 110 cm. The RGA TOFs of the doubly ionized-atomic-oxygen ($M/e = 8$) and rare-gas components are used to obtain velocity distribution functions for beam atoms only. Direct-beam O_2 cannot be measured because of very rapid recombination of AO on ion-source surfaces. Figure 4 shows $M/e = 8$ TOF data points plotted along with the chopper shutter function and the fit to the data resulting from the velocity distribution shown in Fig. 5. The relative composition of the beam cannot be measured using the RGA employed for high-resolution TOF, again because of the rapid recombination of AO into O_2 on ion-source surfaces. A rotatable mass-spectrometer detector in the main scattering chamber that has a flythrough ion source is therefore employed for relative beam composition measurements: the ion source has no grid wire or lens element surface on which recombination can occur. This detector is not employed for high-resolution TOF measurements because of the short path length (25 cm) over which the modulation can expand. The beam composition measurement problem is illustrated by the fact that the flythrough detector shows an O_2 content of ≈1–2% of the total beam flux whereas the high-resolution RGA detector indicates a 30–50%. The TOF detector O_2 wave form is very distorted in comparision with the $M/e = 8$ AO modulation, consistent with AO recombination.

Taking into consideration the Jacobian[13] for the transformation from time to velocity space (t^2), the flux velocity distribution $P(v)$, is found, which, when convoluted with the chopping shutter function, produces a least-squares fit to the laboratory data. Translational energy distributions $P(E)$ are then calculated from $P(v)$ using the Jacobian $(1/v)$ for transformation from velocity to energy space. These laboratory beam distributions are shown in Fig. 5. For comparison, calculated on-orbit velocity and collision energy distributions are shown in Fig. 6. The orbital $P(v)$ is calculated by performing a vector addition of the 8-km/s orbital velocity of the spacecraft with the local Maxwell–Boltzmann gas velocity distribution.

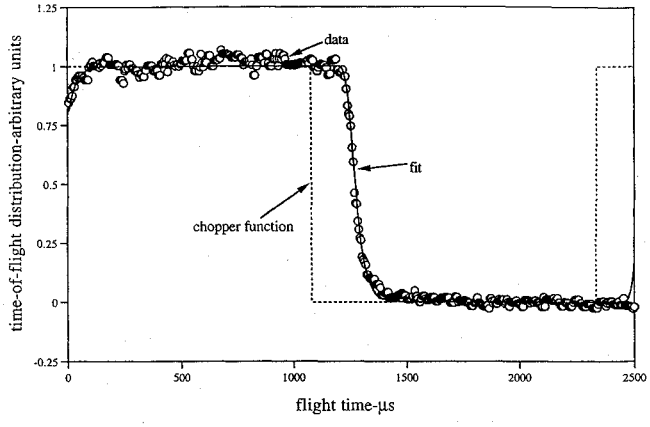

Fig. 4 AO beam-chopper modulation function and least-squares fit of velocity distribution to time-of-flight data.

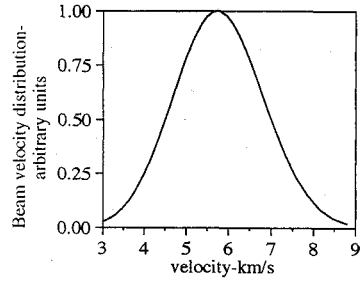

a) AO translational velocity distribution

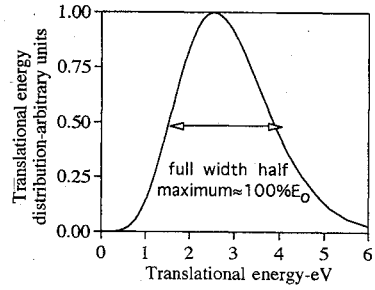

b) AO translational energy distribution

Fig. 5 Best-fit velocity distribution to laboratory data and computed translational kinetic energy distribution.

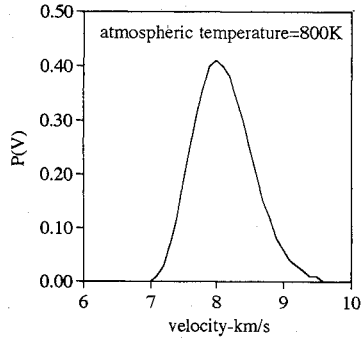

a) Orbital ram AO velocity distribution

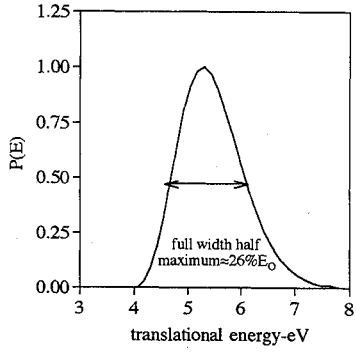

b) Orbital ram AO translational energy distribution

Fig. 6 Calculated orbital AO velocity distribution and resulting translational kinetic energy distribution.

Note that the local temperature of the orbital distribution is $\approx\frac{1}{4}$ that of the laboratory simulation beam.

The relative fluxes of beam species determined by time-of-flight velocity analysis must be converted to absolute fluxes in units of atoms $\cdot$ s^{-1} $\cdot$ cm^{-2} for calibration of the EOIM-III mass spectrometer. The conversion is accomplished by a simple mass balance. When the accommodation chamber (Fig. 2) is isolated from its turbopump, gaseous species can enter and leave the chamber only through the entrance aperture. The total number of atoms of a given type entering the chamber in the high-velocity beam is equal to the total

number leaving as thermalized gases in the limit of free molecular flow:

$$\text{Flux}_{\text{beam}} = \text{flux}_{\text{thermal}} = \frac{1}{4}\sum_i \rho_i \varpi_i \qquad (1)$$

where ρ_i are the partial number densities of the thermalized mixture produced by the atomic oxygen beam in the calibration chamber, and ϖ_i is the most probable thermalized velocity of species i calculated from the chamber temperature T and species mass M, i.e., $(8\,kT/pi\,M)^{1/2}$. The background-corrected partial pressures of the various thermalized beam gases and their reaction products are determined with the RGA positioned out of the direct beam and operated in normal RGA mode, with the calibration-chamber turbopump gated off. The effusive flux of each thermalized product can be easily calculated from gas kinetics and molecular-beam theory,[14] given partial-pressure data, using Eq. (1). A measurement of the absolute total pressure in the calibration chamber with the turbopump valved off provides the final necessary data to calculate the absolute beam flux. For the unreactive inert gases, the effusive flux out of the accommodation chamber is equal to the high-velocity inert-gas flux into the chamber. Knowing the ratio of AO to inert-gas fluxes in the beam provides the necessary information to calculate the beam flux of highly reactive AO.

C. Mass-Spectrometer Calibration

Accurate measurement of the relative densities of various species in the high-velocity beam and the partial pressures (densities) of the thermalized products are fundamental to beam characterization and to the whole mass-spectrometer calibration process. The RGA and the EOIM-III mass spectrometer were calibrated against a molecular-drag gauge. The use of the molecular-drag gauge as a secondary reference standard has been described elsewhere.[15] The thermal-gas calibration spectra were used in several ways. Thermal-gas sensitivity factors for the RGA were used in beam characterization as described above (the AO sensitivity factor was calculated by multiplying the measured rare-gas factor by the ratio of the electron impact ionization cross sections[16] for rare gas and oxygen; the change in velocity on going to the high-energy beam from the thermal-gas was about the same for all beam species). In addition to providing sensitivity factors for thermalized scattering/reaction products, the thermal-gas calibration spectra taken with the EOIM-III mass-spectrometer provide cracking patterns needed to correct the mass-16 signal for contributions from thermalized reaction-product cracking.

High-energy beam calibrations of the EOIM-III mass-spectrometer began with beam characterization as described. EOIM-III calibration spectra were then collected with the calibration chamber turbopump on and the high-energy beam entering the chamber. Background spectra were taken with the beam blocked in the calibration vacuum chamber. Additional spectra were then taken to look for the formation of thermalized reaction products in the EOIM-III itself and to determine the effects of thermal-gas density on the measurement. Comparing the calibration spectra with one produced by blocking the beam with the mass-spectrometer flag provided information about production of thermalized reaction products within the EOIM-III mass spectrometer. On closing the gate valve to the accommodation-chamber turbopump, the high-energy beam produces a pressure rise from roughly 5 to 50 μTorr. EOIM-III mass spectra were taken at both pressures for comparison. Nitrogen was also added to the accommodation chamber with the turbopump on in an alternative approach to evaluating the extent of thermal-gas density effects that exist in LEO.

Calibration spectra were photobackground-corrected (discussed later) by subtracting the average signal between 0.9 and 1.9 amu. Vacuum background spectra were subtracted from photobackground-corrected high-energy beam spectra to produce calibration spectra. Mass-peak areas were calculated for masses 16, 18, 28, 32, 20, 40, and 44. The mass-16 peak was corrected for contributions from water and molecular-oxygen cracking. The correction was determined from cracking patterns of the thermal gases. At mass 16, CO and CO_2 did not produce significant fragment peaks. The high-energy beam sensitivity factor of the EOIM-III mass spectrometer for AO was then calculated by dividing the high-velocity beam AO flux by the corrected mass-16 peak area current in amperes.

III. Results and Discussion

In this section, the general performance characteristics of the EOIM-III mass spectrometer in the high-energy beam calibration system are presented along with quantitative calibration results. The results of experiments designed to evaluate the effects of differences between the calibration system environment and the LEO environment are also reported.

The high-energy atom-beam source produces a significant flux of uv and vacuum uv (vuv) photons. Scattering of these photons in the EOIM-III mass-spectrometer produces large photocurrents in the instrument output, which are corrected by subtracting the average signal in a part of the spectrum which contained no mass-peak features. Photobackgrounds between 0.2 and 0.5 nA are typical (see Figs. 7 and 8). Because optical spectra of the beam source show that the beam source produces about 2 equivalent vacuum uv (vuv) suns in the uv-vuv region,[11] similar effects are expected if the EOIM-III spectrometer becomes aligned with the sun during the EOIM-III flight experiment. The photobackground is surprising in that the EOIM-III mass-spectrometer is designed with an off-axis ion multiplier, i.e., the photon source is not line-of-sight to the detector. However, a fine gold screen covers the ion exit aperture, and scattering of photons from the screen into the electron-multiplier detector is the most likely explanation for the photobackground.

The EOIM-III mass spectrometer is not an ultrahigh-vacuum instrument. It contains significant quantities of AO-reactive organic materials and cannot be baked out above about 150°C. As a result, introduction of the high-velocity atom beam always produces large thermalized scattering/reaction product signals formed by reaction of AO with organic materials in the mass spectrometer itself and O_2 from recombination of AO on surfaces of the mass spectrometer. Figure 7 shows a typical high-velocity beam spectrum taken shortly

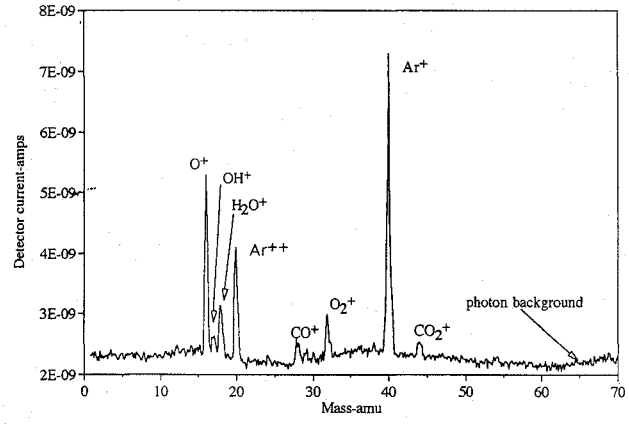

Fig. 7 Laboratory mass spectrum of 50% argon, 50% AO beam taken with flight mass spectrometer under low-fluence condition.

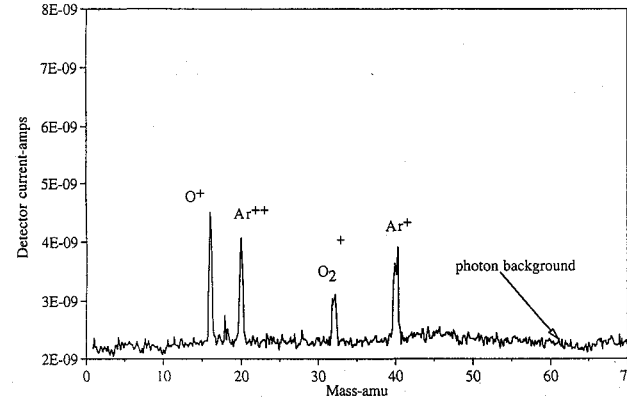

Fig. 8 Laboratory mass spectrum of 50% argon, 50% AO beam taken with flight mass spectrometer under high-fluence condition.

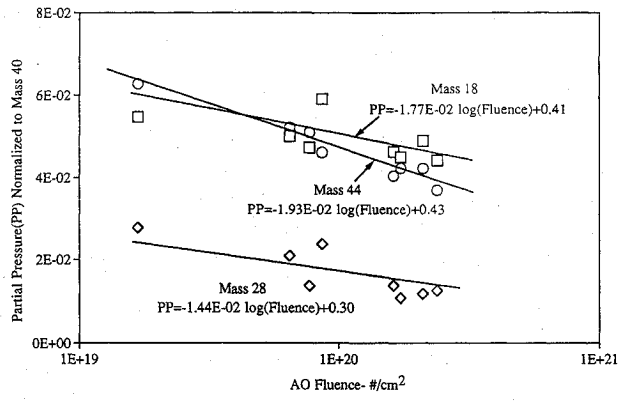

Fig. 9 H_2O, CO, and CO_2 partial ion currents as a function of AO fluence.

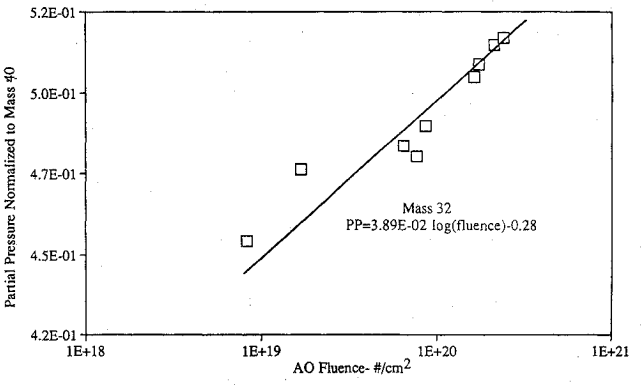

Fig. 10 O_2 partial ion current as a function of AO fluence.

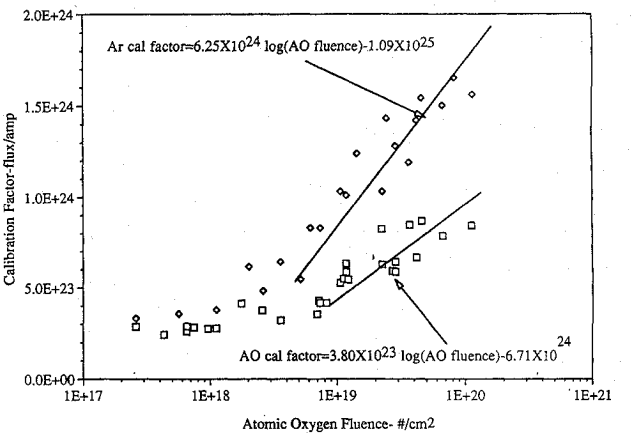

Fig. 11 Atomic-oxygen calibration factor as a function of AO fluence.

after the AO beam entered the instrument (low-fluence data). Note the photo-ion current background and thermalized H_2O, CO, CO_2, and O_2 mass peaks. Figure 8 shows the mass spectrum recorded after many hours of AO beam exposure. Note that both Figs. 7 and 8 are plotted on the same linear vertical scale; that the peaks for thermalized reaction products have been greatly reduced (Fig. 8), leaving only recombined O_2; and that the sensitivity of the instrument has gone down, i.e., even though the AO beam flux is constant to within 2–3% and the ionizing electron current is trap-regulated, the mass-16 (O^+) and mass-40 (Ar^+) peaks have decreased substantially. Note also that the photo-ion current background has not changed to any appreciable extent, indicating that the ion-multiplier detector sensitivity had not changed. As will be shown in other publications, this same effect has been observed on orbit.

The beam flag experiments show that most of the mass-16 signal arises from AO in the high-energy beam and that most of the H_2O, CO, and CO_2 and all the O_2 forms inside the EOIM-III mass-spectrometer. There are two processes operating to reduce mass-analyzed ion signals in this instrument. First, there appears to be a mass-independent decrease in instrument sensitivity to all mass-analyzed signals, but not to the photoproduced ion signal. In addition, the decrease in sensitivity is reversible, i.e., if the instrument is allowed to remain unused for several days, the original sensitivity is recovered and subsequently decreases during AO exposure. These effects rule out a change in electron-multiplier sensitivity, which is always permanent, and changes in ion-source electron emission are ruled out because the emission is electron-trap-regulated. Secondly, the reaction product peak intensities decrease because of cleanup of the instrument, over and above the decrease in overall instrument sensitivity. Figure 9 shows the variation of the reaction products, intensity with AO fluence, normalized to the argon peak intensity. This demonstrates the net cleanup effect of the AO beam. Note that the plot is logarithmic in fluence, so that a leveling off of the reaction-product decrease is indicated. Figure 10, however, shows the increase in O_2 number density as the hydrocarbon surface contaminants are cleaned up. Again the mass-32 signal has been normalized to the argon gas intensity to remove the effect of instrument sensitivity change. Both of these effects show an induction period up to a fluence of $\approx 10^{19}$ AO/cm^2 in which the peak intensities do not change with fluence. If a reactivity of a polyimide (3×10^{-24} cm^3/atom) is assumed for the contaminant, and the induction period is assumed to be caused by the burnoff of the contaminant, then the amount of hydrocarbon is of the order of 1500 to 3000 Å (50 to 100 monolayers) thick. Flowing afterglow experiments[17] involving AO have revealed anomalous sensitivity changes with exposure to AO. The instruments used in these experiments have a small pinhole isolating the mass-spectrometer quadrupole from the ionization region, very similar to the present arrangement. It was found that changes in the pinhole produced dramatic changes in the mass spectral intensity. The type of material that the pinhole was made from was important. Material such as graphite gave the most stable operation, and gold and stainless steel gave the greatest changes in intensity. These reports are consistent with our findings that as carbon contaminants are removed from the instrument, intensity changes are the greatest. Oxides most likely form on clean pinhole surfaces, which subsequently must alter electrostatic focusing fields. The precise mechanism is not known or understood.

The high-energy AO calibration results for the EOIM-III mass spectrometer are shown in Fig. 11. Since the sensitivity of the instrument changes with fluence, the calibration factor that relates the mass-16 and mass-40 ion currents to input flux must also have a fluence dependence. The average AO calibration factor during the induction period is $(2.7 \pm 1) \times 10^{23}$ (atoms · cm^{-2} · s^{-1})/A, and that for argon was 3.52×10^{23}. The oxygen atom flux varied from 3×10^{14} to 3×10^{15} atoms · cm^{-2} · s^{-1} and the velocity varied from 3.0 to 5.3 km/s, and total flux of all beam species varied from 2.7×10^{15} to 7.1×10^{15} atoms · cm^{-2} · s^{-1}. The calibration factor appears to change as the logarithm of fluence after an induction period of $\approx 10^{19}$ AO/cm^2.

The calibration factor showed no significant correlation with beam velocity, oxygen atom flux, total flux, and total pressure, but did show a strong dependence on oxygen atom fluence. The fluence dependence was reversible and correlated with the state of cleanliness of the instrument, i.e., with high levels of reactive products, the instrument sensitivity was high (low calibration factor). The lack of correlation with oxygen atom flux and total pressure (nitrogen or beam gas) is not surprising, because the EOIM-III mass spectrometer produces linear response over a wide pressure (density) range. The lack of a detectable correlation with velocity is not surprising either, because the source is of the open type, i.e., the source detects both thermalized and direct flux components. The high-velocity beam itself produces a density in the ionizer on the order of 6×10^9 atoms · cm^{-3}. At the typical calibration pressure of 5×10^{-6} Torr, the thermal-gas density throughout the accommodation chamber (including the ionizer) is on the order of 2×10^{11} cm^{-3}, implying that the high-velocity beam density is only about 4% of the total density. Yet the data show the high-velocity beam species as a significant part of the total gas density, even without the use of atom-beam modulation and phase-sensitive detection. The concept of ram density resolves the apparent paradox. At steady state, the number

of high-velocity atoms and molecules entering the ion source in the high-velocity beam must equal the number of thermalized species leaving, i.e.,

$$\rho_{\text{beam}} v_{\text{beam}} = \rho_{\text{thermal,ram}} v_{\text{thermal}} \quad (2)$$

$$\rho_{\text{beam}} / \rho_{\text{thermal,ram}} = v_{\text{thermal,ram}} / v_{\text{beam}} = 0.1 \quad (3)$$

at the ion source entrance, where ρ is the gas density and v is the gas velocity. Clearly, the ram-density effect can produce a 10-fold enhancement in the total density of any species found in the high-velocity beam if that species can survive thermalization. The fact that the calibration factor shows very little atom-velocity dependence can be explained if the atomic oxygen detected by the EOIM-III mass-spectrometer is thermalized, ram-density AO, with a half-life against reaction and escape that is long enough to permit detection. Preliminary beam modulation experiments suggest that AO has an ion-source half-life shorter than that of Ar, H_2O, CO, or CO_2, but still long enough to permit detection as a thermalized gas.

IV. Summary and Conclusions

Calibration of the EOIM-III flight mass-spectrometer has shown the feasibility of providing important insights into the operating characteristics of flight instruments, which heretofore had not been possible for lack of a hyperthermal cw AO ground-based facility. High-velocity beam calibration experiments have shown that the calibration factor is not stable when exposed to highly reactive hyperthermal AO. This appears to be due to a little-understood phenomenon discovered in flowing afterglow experiment of surface oxidation. In the case of the current instrument, the phenomenon is reversible, i.e., after the instrument becomes contaminated with hydrocarbon deposits, the sensitivity returns to a high value. One of the problems in studying this phenomenon is that there is no good quantitative diagnostic for the amount of surface contamination. Therefore, successive calibration runs may have differing induction periods, or an induction period may not be observable because of too little instrument contamination. No significant correlation, however, was found with background-gas identity or pressure, beam velocity, or beam flux. Significant amounts of H_2O, CO, O_2, and CO_2 were produced in the EOIM-III mass-spectrometer whenever the high-energy beam entered the ion source, and the intensity of these products decreased with time as the instrument cleaned up. Beam-flag experiments show that AO reacts with the EOIM-III mass-spectrometer surfaces to produce the reaction products and that extensive recombination of AO to molecular oxygen occurs as the instrument becomes cleaner.

Ion-source gas density calculations, the absence of a correlation between calibration factor and atom-beam velocity, and the intensity of the mass spectral peaks produced during the beam calibration experiments point to the mechanism of interaction between the EOIM-III flight mass spectrometer and the high-velocity atom beam. High-velocity beam species are detected as a thermalized "ram density" gas after collision with mass-spectrometer surfaces. The EOIM-III flight mass spectrometer is an open-source instrument in which the contribution to the mass spectrum of those beam species with full beam velocity is negligible.

On orbit, the principal ram species are AO and molecular nitrogen entering the flight mass spectrometer with a velocity of 8 $\text{km} \cdot \text{s}^{-1}$. In the calibration system, AO, molecular oxygen, and argon or neon enter the mass spectrometer at velocities between 3 and 6 $\text{km} \cdot \text{s}^{-1}$. The lack of correlation between atom velocity and calibration factor, and the measurement mechanism implied, suggest that the difference between orbital velocity and calibration-system velocity is relatively unimportant. The lack of any correlation with background pressure or background-gas identity further supports the conclusion that the existing calibration is valid in the orbital environment.

Acknowledgment

Financial support of the Los Alamos effort from Johnson Space Flight Center is gratefully acknowledged.

References

[1]Visentine, J. T., and Leger, L. J., "Material Interaction with the Low Earth Orbital Environment: Accurate Reaction Rate Measurements," in *Proceedings of the NASA Workshop on Atomic Oxygen Effects*, edited by D. E. Brinza, Jet Propulsion Lab., Publication 84-14, 1987, pp. 11–20.

[2]Hunton, D. E., Trzeinski, E., Cross, J. B., Spangler, L. H., Hoffbauer, M. A., Archuleta, F. H., and Visentine, J. T., "Mass Spectrometers and Atomic Oxygen," *Proceedings of the NASA Workshop on Atomic Oxygen Effects*, edited by D. E. Brinza, Jet Propulsion Lab., Publication 84-14, 1987, pp. 21–28.

[3]Hedin, A. E., *High Altitude Atmospheric Modeling*, NASA 100707, Oct. 1988.

[4]Leger, L. J., Spiker, I. K., Kuminecz, J. F., Ballentine, T. J., and Visentine, J. T., "STS-5 LEO Effects Experiment—Background Description and Thin Film Results," AIAA Paper AIAA-83-2631, 1983.

[5]Visentine, J. T., Leger, L. J., Kuminecz, J. F., and Spiker, I. K., "STS-8 Atomic Oxygen Effects Experiment," AIAA Paper 85-0415, 1985.

[6]Zimcik, D. G., and Maag, C. R., "Results of Apparent Atomic Oxygen Interactions with Spacecraft Materials During Shuttle Flight STS-41G," *Journal of Spacecraft and Rockets*, Vol. 25, No. 2, 1988, pp. 162–167.

[7]Clark, L. G., Kinard, W. H., Carter, D. J., and Jones, J. L., "The Long Duration Exposure Facility," NASA SP-473, March 1984.

[8]Ballenthin, J. O., and Nier, A. O., "Molecular Beam Facility for Studying Mass Spectrometer Performance," *Review of Scientific Instruments*, Vol. 52, No. 7, 1981, pp. 1016–1024.

[9]Hayden, L. J., Nier, A. O., French, J. B., Reid, N. M., and Ducket, R. J., "The Characteristics of an Open Source Mass Spectrometer Under Conditions Simulating Upper Atmosphere Flight," *International Journal of Mass Spectrometry and Ion Physics*, Vol. 15, 1974, pp. 37–47.

[10]Cross, J. B., and Blais, N. C., "High Energy/Intensity Atomic Oxygen Beam Source," *Rarefied Gas Dynamic: Space-Related Studies*, edited by E. P. Muntz, D. P. Weaver, and D. H. Campbell, Progress in Astronautics and Aeronautics, Vol. 116, AIAA, Washington, DC, 1989.

[11]Hunton, D. E., Trzcinski, E., Wlodyka, L., Federico, G., and Dorian J., *Quadrupole Ion/Neutral Mass-Spectrometer (for Space Shuttle Applications)*, AFGL-TR-86-0084, Air Force Geophysics Lab., Hanscomb AFB, MA, April 1987.

[12]Cross, J. B., Koontz, S. L., Gregory, J. C., and Edgell, M. J., "Hyperthermal Atomic Oxygen Reactions with Kapton and Polyethylene," *Materials Degradation in Low Earth Orbit (LEO)*, edited by B. A. Banks and V. Srinivasan, The Minerals, Metals and Materials Society, Warrendale, PA, 1990, pp. 1–13.

[13]Levine, R. D., and Bernstein, R. B., *Molecular Reaction Dynamics*, Oxford Univ. Press, New York, 1974.

[14]English, T. C., and Zorn, J. C., "Molecular Beam Spectroscopy," *Methods of Experimental Physics—Molecular Physics*, 2nd ed., Vol. 3, edited by D. Williams, Academic, New York, 1974, pp. 669–846.

[15]Dittmann, S., Lindenau, B. E., and Tilford, C. R., "The Molecular Drag Gauge as a Calibration Standard," *Journal of Vacuum Science and Technology A*, Vol. 7, No. 6, 1989, pp. 3356–3361.

[16]Kieffer, J. L., and Dunn, G. H., "Electron Impact Ionization Cross Section Data for Atoms, Atomic Ions, and Diatomic Molecules: I. Experimental Data," *Reviews of Modern Physics*, Vol. 38, No. 1, 1966, pp. 1–35.

[17]Fergeson, E. E., Feshenfeld, F. C., and Schmeltenkoph, A. L., "Flowing Afterglow Measurements of Ion-Neutral Reactions," *Advances in Atomic and Molecular Physics*, Vol. 5, edited by D. R. Bates and I. Estermann, Academic, New York, 1969, pp. 12, 13.

R. K. Clark
Associate Editor